NANO LETTERS

Letter

pubs.acs.org/NanoLett

Out-of-Plane Electromechanical Response of Monolayer Molybdenum Disulfide Measured by Piezoresponse Force Microscopy

Christopher J. Brennan,[†,‡] Rudresh Ghosh,[†,‡] Kalhan Koul,[†,‡] Sanjay K. Banerjee,[†,‡,§] Nanshu Lu,[*,†,‡,§,∥,⊥] and Edward T. Yu[*,†,‡,§]

[†]Microelectronics Research Center, University of Texas at Austin, Austin, Texas 78758, United States

[‡]Department of Electrical and Computer Engineering, University of Texas at Austin, Austin, Texas 78701, United States

[§]Texas Materials Institute, University of Texas at Austin, Austin, Texas 78712, United States

[∥]Center for Mechanics of Solids, Structures, and Materials, Department of Aerospace Engineering and Engineering Mechanics, University of Texas at Austin, Austin, Texas 78712, United States

[⊥]Department of Biomedical Engineering, University of Texas at Austin, Austin, Texas 78712, United States

S *Supporting Information*

ABSTRACT: Two-dimensional (2D) materials have recently been theoretically predicted and experimentally confirmed to exhibit electromechanical coupling. Specifically, monolayer and few-layer molybdenum disulfide (MoS_2) have been measured to be piezoelectric within the plane of their atoms. This work demonstrates and quantifies a nonzero out-of-plane electromechanical response of monolayer MoS_2 and discusses its possible origins. A piezoresponse force microscope was used to measure the out-of-plane deformation of monolayer MoS_2 on Au/Si and Al_2O_3/Si substrates. Using a vectorial background subtraction technique, we estimate the effective out-of-plane piezoelectric coefficient, d_{33}^{eff}, for monolayer MoS_2 to be 1.03 ± 0.22 pm/V when measured on the Au/Si substrate and 1.35 ± 0.24 pm/V when measured on Al_2O_3/Si. This is on the same order as the in-plane coefficient d_{11} reported for monolayer MoS_2. Interpreting the out-of-plane response as a flexoelectric response, the effective flexoelectric coefficient, μ_{eff}^{*}, is estimated to be 0.10 nC/m. Analysis has ruled out the possibility of elastic and electrostatic forces contributing to the measured electromechanical response. X-ray photoelectron spectroscopy detected some contaminants on both MoS_2 and its substrate, but the background subtraction technique is expected to remove major contributions from the unwanted contaminants. These measurements provide evidence that monolayer MoS_2 exhibits an out-of-plane electromechanical response and our analysis offers estimates of the effective piezoelectric and flexoelectric coefficients.

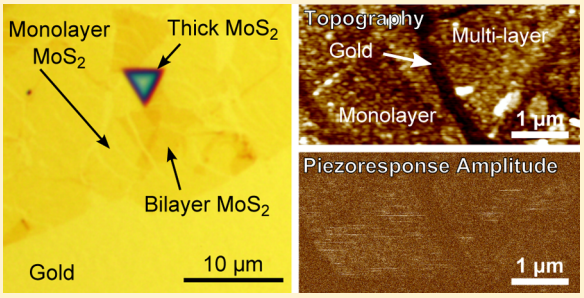

KEYWORDS: *MoS_2, electromechanical coupling, flexoelectricity, piezoelectricity, piezoresponse force microscopy*

The coupling of electronic and mechanical behaviors in crystalline materials has created many engineering opportunities. Strain is commonly used in electronics to alter electronic bandgaps and carrier mobilities,[1] and electromechanical coupling is widely used in microelectromechanical systems (MEMS) to make sensors,[2] actuators,[3] and generators.[4] One of the most widely used electromechanical coupling phenomena is piezoelectricity, which links crystal polarization and mechanical strain. Piezoelectricity only exists in noncentrosymmetric crystalline materials, limiting the range of possible materials to use for such applications. As scaling trends continue to shrink the feature size of materials, a need arises for nanoscale piezoelectric materials. Two-dimensional (2D) materials are very popular candidates for nanodevices because of their exotic electronic properties,[5] transparency,[6,7] and mechanical robustness,[8] and have recently be shown to be candidates for electromechanical nanotransducers.[9,10]

In the atomically thin limit, transition metal dichalcogenides (TMDs) are intrinsically piezoelectric due to the lack of inversion symmetry in their crystal structure.[11] Piezoelectricity arises within the plane of their atoms and both direct[9,12] and converse[12,13] piezoelectric effects have been experimentally confirmed in monolayer and few layer molybdenum disulfide (MoS_2). In-plane piezoelectricity should only exist in odd-number layers of TMDs where there is no inversion symmetry present and decrease rapidly as the number of layers increases due to cancellation of the responses from oppositely oriented layers.[9] Any strain or electric field applied perpendicular to the surface of the MoS_2 will theoretically yield zero piezoelectric response due to its crystal symmetry.

Received: May 19, 2017
Revised: July 25, 2017
Published: August 1, 2017

DOI: 10.1021/acs.nanolett.7b02123
Nano Lett. XXXX, XXX, XXX−XXX

Piezoelectricity is, however, only one type of electromechanical response possible in crystal lattices. In flexoelectricity, polarization arises from strain gradients as opposed to uniform strain.[14−16] Thus, a fourth-order tensor describes flexoelectricity, while a third-order tensor describes piezoelectricity. With an even-rank tensor, flexoelectricity is present in every crystal class. Despite this, flexoelectricity has been seldom studied because the strain gradients necessary to cause a noticeable change in polarization in macro-scale materials requires very large strains that can fracture the material. However, in nanoscale materials even small strain can cause large gradients to form.

Investigations of flexoelectricity in 2D materials[16−18] have mainly focused on either carbon systems[19−21] or hexagonal boron nitride.[22,23] These works were performed from the modeling side but since 2D materials are the ultimate nanoscale material and can have large strain gradients they can offer a platform for experimental studies of flexoelectricity.

Another reason for the lack of experimental study of flexoelectricity is because piezoelectricity and flexoelectricity are difficult to isolate from each other. We propose a solution to this problem by utilizing the symmetry of MoS_2 and other TMDs. Their crystal class, D_{3h} ($\bar{6}m2$), results in a flexoelectric tensor that has nonzero coefficients in the out-of-plane direction,[24] whereas all out-of-plane piezoelectric coefficients are zero.[11] Flexoelectricity in 2D materials can therefore be studied experimentally if an out-of-plane electromechanical response in MoS_2 is measurable. There have been a few notable experimental studies investigating out-of-plane electromechanical properties of 2D materials, namely on graphene-nitride nanosheets with nonsymmetric holes[25] and graphene forming bonds to the underlying SiO_2 substrate.[26] Neither study suggested an estimate for a flexoelectric coefficient. Interestingly, because 2D materials are essentially only a surface, it becomes ambiguous whether out-of-plane electromechanical effects caused by spatial gradients should be referred to as flexoelectricity or surface piezoelectricity.[14,15] Nevertheless, it is referred to as a flexoelectric response here.

Piezoresponse force microscope (PFM) is used to measure out-of-plane electromechanical deformation resulting from an applied out-of-plane electric field. Because an electric field is inducing a strain, this is referred to as the converse piezoelectric effect; the direct piezoelectric effect is a strain inducing a polarization. In the measurement, an atomic force microscope (AFM) with a conductive probe is used to apply an electric field through the test material by applying a drive voltage, V_d, between the tip and substrate. If there is electromechanical coupling in the material, the AFM tip will be deflected by the expansion and contraction of the material. A lock-in amplifier is used to measure both the amplitude and phase of the response while simultaneously measuring surface topography. (See Figure S1 in the Supporting Information for details regarding the PFM measurement and tip−sample geometry.)

The quantity usually obtained from PFM experiments, d_{33}, is the piezoelectric coefficient that represents the out-of-plane piezoelectric response created by an out-of-plane electric field (see Supporting Information Note 1 for details on calculating d_{33} from PFM signals). In actual PFM experiments, the measurement should be referred to as an effective value, d_{33}^{eff}, because of additional possible contributions to the signal including material clamping,[27] inhomogeneous field effects,[28] and other electromechanical effects. Other factors that may affect the measurement and introduce experimental uncertainty include electrostatic effects,[29] topographic artifacts,[30] cantilever dynamics,[31,32] and instrumental noise.[32]

To help minimize the contribution of nonelectromechanical effects and obtain a quantitative estimate of the true electromechanical response of the test material, a vectorial background subtraction technique is used.[33,34] PFM measurements taken on nonpiezoelectric substrates or without applying V_d serve as two different measurements of the background contribution to the measured MoS_2 signal. These measurements, which have an amplitude and phase component, can then be made into vectors. Next, by performing a vector subtraction of the background signal from the MoS_2 signal, a more accurate representation of d_{33}^{eff} can be obtained. The details of this process will be illustrated with data later in this paper.

Samples are made by transferring CVD grown MoS_2 from a growth substrate to either 70 nm gold (Au) or 5.3 nm alumina (Al_2O_3) deposited on an n^{++} silicon substrate. Detailed sample preparation steps are described in the Methods as well as Figure S2. The Au is used to concentrate the electric field within the MoS_2 and serves as the bottom electrode. The Al_2O_3 serves as a dielectric layer to limit current flow with the n^{++} Si substrate now acting as the bottom electrode. Figure 1 shows a schematic

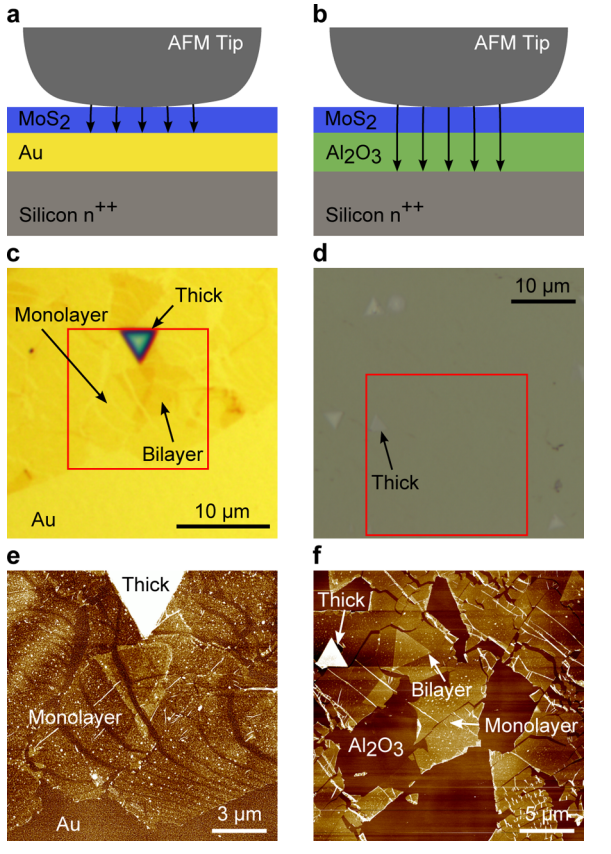

Figure 1. Schematics of the two samples: (a) MoS_2 on 70 nm Au on n^{++} Si and (b) MoS_2 on 5.3 nm Al_2O_3 on n^{++} Si. The black arrows indicate the electric field coming from the AFM tip terminating at the conductive substrates. Because the MoS_2 is monolayer, the AFM tip radius will appear broad in comparison. Optical images of the MoS_2/Au/Si sample (c) and MoS_2/Al_2O_3/Si sample (d) show that the MoS_2 is optically visible on Au but not on the Al_2O_3/Si substrate. Tapping mode AFM images of the MoS_2/Au/Si sample (e) and the MoS_2/Al_2O_3/Si sample (f) show that the monolayer and multilayer MoS_2 layers can be clearly distinguished from the substrate.

DOI: 10.1021/acs.nanolett.7b02123
Nano Lett. XXXX, XXX, XXX−XXX

of the two sample types, along with optical and tapping-mode AFM images of each. The Al_2O_3/Si sample has very limited optical contrast, resulting in very weak Raman and photoluminescence (PL) signals.[35] In this case, tapping-mode AFM was used to identify locations of MoS_2. Figure 2 shows Raman data taken at different locations on each sample. On the Au sample (Figure 2a), the separation of the E^1_{2g} and A_{1g} peaks for MoS_2 increases from 19.7 to 25.7 cm^{-1} from monolayer to thick MoS_2, and both peaks increase in intensity, which is consistent with observations reported in the literature.[36] Only the thick MoS_2 yields measurable Raman data on the Al_2O_3/Si sample (Figure 2b) with a peak separation of 26.1 cm^{-1}. The peak near 520 cm^{-1} is from the underlying silicon. Further discussion of MoS_2 thickness and weak Raman and PL data is provided in Supporting Information Note 2 and Figures S3–S5. PL and Raman measurements at different steps of sample preparation are shown in Figure S6, revealing that residual tensile strain caused during growth is released during the transfer process.

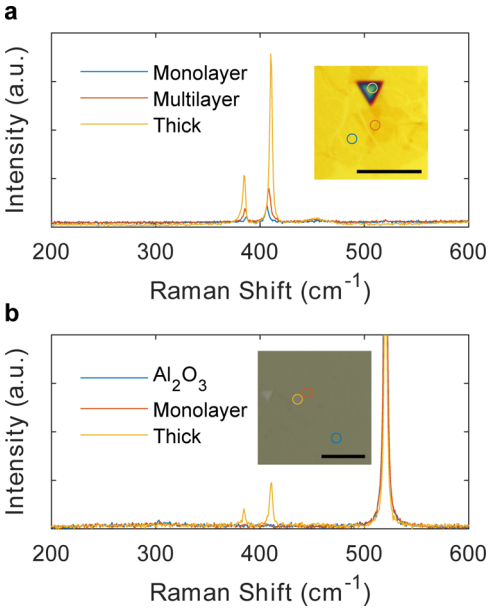

Figure 2. Raman measurements of (a) MoS_2/Au/Si and (b) MoS_2/Al_2O_3/Si samples. The areas measured are circled in the inset microscope images with corresponding colors. The scale bars are 10 μm. The intensity of the MoS_2 Raman signals increases as thicker layers are measured. The peak separation also increases as the thickness increases, as expected. Only the thick MoS_2 region on the Al_2O_3 sample gives a detectable Raman signature due to poor optical absorption caused by the substrate.

Figure 3 shows PFM images of MoS_2 on Au. The topographic (Figure 3a), piezoresponse (PR) amplitude (Figure 3b), and PR phase (Figure 3c) channels with V_d applied show that there is clear contrast between the MoS_2 and the Au. When the voltage is not applied, contrast in topography remains (Figure 3d) whereas contrast in piezoresponse disappears (Figure 3e,f), allowing topographic artifacts to be ruled out.

By using the values measured on Au and those measured without the voltage applied as two separate background signals in the vectorial background subtraction process, we obtain the out-of-plane effective piezoelectric coefficient of MoS_2. As illustrated in Figure 4, with the amplitude and phase information, the measured PR of MoS_2 on Au (black) and the measured PR of the Au background (red) are plotted as two vectors in a 2D x–y graph. In both cases, an average of the amplitude and phase data taken over an area of only monolayer MoS_2 or the Au substrate is done to obtain the two vectors. The difference between the two vectors (blue) is taken to be the true PR coming from the MoS_2. More details of the vectorial background subtraction method can be found in Supporting Information Note 3. The background-subtracted PR can then be converted to a d^{eff}_{33} value using the deflection sensitivity of the cantilever and the drive voltage (details given in Supporting Information Note 1). We finally obtain 0.93 ± 0.23 and 1.12 ± 0.20 pm/V for d^{eff}_{33} of MoS_2 using the Au and the voltage-off condition as the background, respectively. The two values are consistent within our experimental uncertainty, reinforcing that there are minimal topographic artifacts, that the Au makes little to no contribution to the PR, and that the PR is truly associated with the presence of the MoS_2. Detailed analysis of the uncertainty is given in Supporting Information Note 4. In comparison, a piezoelectric lithium niobate ($LiNbO_3$) reference sample has a d_{33} of 7.5 pm/V, d_{11} for

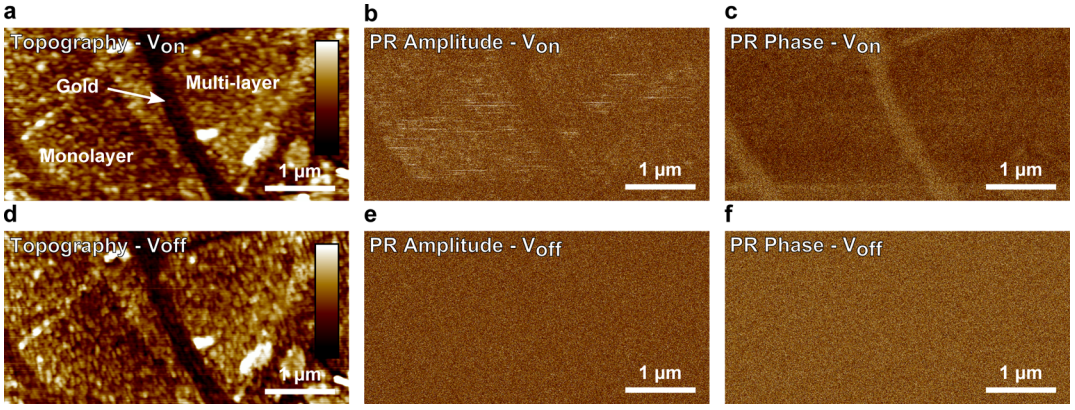

Figure 3. A series of two PFM measurements on the MoS_2/Au sample with the drive voltage applied (V_{on}) (a–c) and not applied (V_{off}) (d–f). The topography images (a,d) show the background Au substrate, monolayer MoS_2, and multilayer MoS_2 regions. The applied drive voltage does not affect the topographic measurement (color bar is 0–5 nm for both). The piezoresonse (PR) amplitude images (b,e) show that the MoS_2 region has contrast against the Au substrate only when the drive voltage is applied (b). The same is true for the PR phase images (c,f). Both amplitude images and phase images share the same color scale.

DOI: 10.1021/acs.nanolett.7b02123
Nano Lett. XXXX, XXX, XXX–XXX

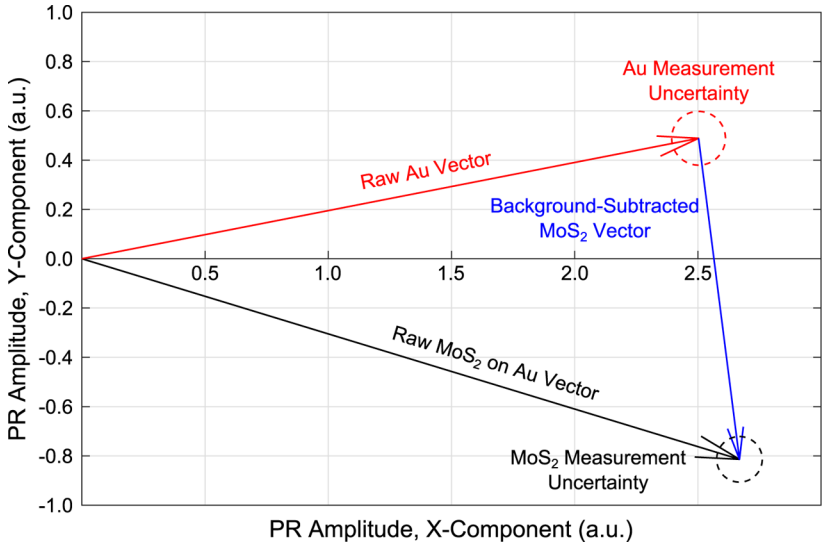

Figure 4. A schematic illustration of how the background subtraction method is performed to calculate d_{33}^{eff}. The amplitude and phase channels of the MoS2 (black) and Au (red) PFM measurements are used to make two separate vectors. The actual signal is the difference between these two vectors (blue). The dashed circles at the end of the vectors represent the uncertainty of the measured amplitudes and phases.

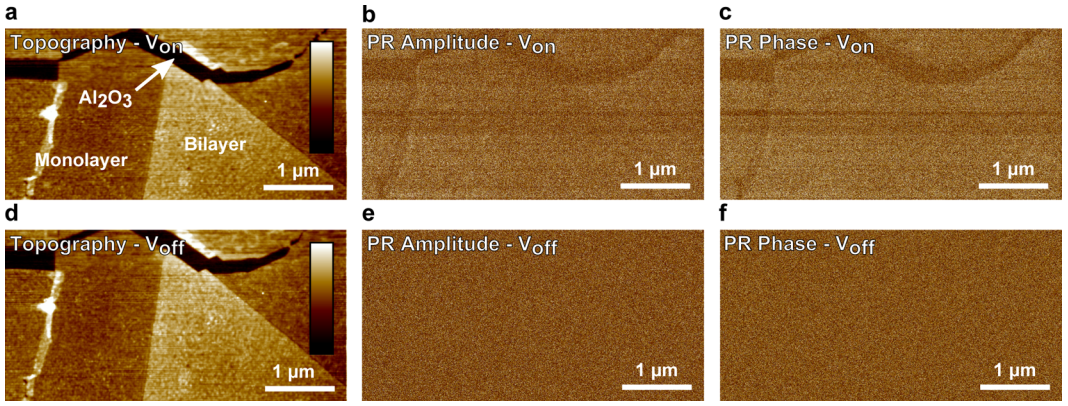

Figure 5. A series of two PFM measurements on the MoS_2/Al_2O_3 sample with the drive voltage applied (V_{on}) (a,b) and not applied (V_{off}) (d–f). The topography images (a,d) show the background Al_2O_3 substrate, monolayer MoS_2, and bilayer MoS_2 regions. The applied drive voltage does not affect the topographic measurement (color bar is 0 to 3.7 nm for both). The PR amplitude images (b,e) show that the MoS_2 region has contrast against the Al_2O_3 substrate only when the drive voltage is applied (b). The same is true for the PR phase images (c,f). Both amplitude images and phase images share the same color scale.

monolayer MoS_2 has been measured[13] to be 1.85 pm/V, and theoretical estimates for d_{11} of MoS_2 range from 2.91 to 3.73 pm/V for clamped- and relaxed-ion cases.[11]

To eliminate the possibility that the observed PR signals are affected by current flow at the tip-MoS_2–Au junction, the Al_2O_3/Si samples were fabricated to limit the potential current flow by introducing an insulating dielectric layer. Figure 5 shows the topographic (Figure 5a), PR amplitude (Figure 5b), and PR phase (Figure 5c) channels of the Al_2O_3/Si sample while V_d is applied. Similar to the case of the Au sample, there are clear differences in the PFM signal on the MoS_2 versus Al_2O_3 when the voltage is applied, but no differences when the voltage is not applied (Figure 5d–f). In this case, an added complication arises because the voltage is being dropped over a larger distance and over two different materials. Given V_d applied between the AFM tip and the n^{++} silicon substrate, the voltage drop across only the MoS_2, V_{MoS_2}, can be estimated using a simple planar capacitance model

$$V_{MoS_2} = V_d \frac{\frac{\epsilon_{Al_2O_3}}{t_{Al_2O_3}}}{\frac{\epsilon_{MoS_2}}{t_{MoS_2}} + \frac{\epsilon_{Al_2O_3}}{t_{Al_2O_3}}} \quad (1)$$

where $\epsilon_{Al_2O_3}$, ϵ_{MoS_2}, $t_{Al_2O_3}$, and t_{MoS_2} are the permittivity of the Al_2O_3 and MoS_2, and the thickness of the Al_2O_3 and MoS_2, respectively (see Supporting Information Note 5). On the basis of the estimated voltage drop, d_{33}^{eff} is calculated to be 1.34 ± 0.27 and 1.35 ± 0.20 pm/V using the Al_2O_3 or the voltage-off condition as the background, respectively. These values are slightly larger than the values measured on Au but are still within our experimental uncertainty. Discrepancies could be caused by variability in the separate AFM tips used, variable wear of the AFM tips, changes caused by the presence or absence of current flow, depletion of carriers in the n^{++} Si bottom electrode, or differences in geometries between the two systems. The results for the two different types of samples are summarized in Table 1. The last column compares the signal

DOI: 10.1021/acs.nanolett.7b02123
Nano Lett. XXXX, XXX, XXX–XXX

measured on the respective substrates to the voltage-off condition, showing that the substrates are not piezoelectric.

Table 1. d_{33}^{eff} and Uncertainty Values Calculated from Preforming Background Subtraction with the Indicated PFM Vectors

	MoS_2 versus Sub (pm/V)	MoS_2 versus V_{off} (pm/V)	Sub versus V_{off} (pm/V)
Au/Si sample	0.93 ± 0.23	1.12 ± 0.20	0.19 ± 0.10
Al_2O_3/Si sample	1.34 ± 0.27	1.35 ± 0.20	0.04 ± 0.15

To understand the origin of the measured d_{33}^{eff} signal in the PFM experiment, including the potential contribution of flexoelectric response, a closer look at the forces involved in the measurement is required. The multiple contributions to the force that acts on the AFM tip can be summarized by

$$F_{tot} = F_0 + F_{ES} + F_{EM} \tag{2}$$

where F_{tot} is the total force, F_0 the elastic force, F_{ES} the electrostatic force, and F_{EM} the electromechanical force. The different force components can be further written as

$$F_0 = kd_0 \tag{3a}$$

$$F_{ES} = F_{ES}^{Tip} + F_{ES}^{Cant} \tag{3b}$$

$$F_{EM} = F_{EM}^{Piezo} + F_{EM}^{Flexo} \tag{3c}$$

where k is the spring constant of the AFM cantilever and d_0 is the deflection set point, that is, the amount of deflection the cantilever experiences while in constant contact with the sample. The electrostatic force is split into contributions from the tip, F_{ES}^{Tip}, and the cantilever, F_{ES}^{Cant}, and the electromechanical force is split into components from piezoelectricity, F_{EM}^{Piezo}, and flexoelectricity, F_{EM}^{Flexo}.

The elastic contribution comes from the PFM measurement being a contact-mode AFM technique. The AFM tip is brought into contact with the sample surface and a constant feedback loop attempts to keep the tip and cantilever at a constant level of deflection, d_0. The constant deflection will create a constant elastic force given by eq 3a. Because the PFM measurement uses a lock-in amplifier which only amplifies signals at the same frequency as the reference signal, the constant elastic force will have no effect on the PFM signal.

However, during the scanning motion, the feedback system will be moving the tip vertically with the topography of the sample to maintain a constant deflection. This gives rise to two possible concerns: (1) the feedback frequencies may interfere with the applied drive frequency, and (2) the tip motion from changing topography could cause topographic artifacts if motion occurs at the same frequency as V_d. A proper V_d frequency is chosen by taking a frequency sweep of the PR amplitude and choosing a frequency within a range which gives a largely frequency-independent PR amplitude (Supporting Information Note 6 and Figure S7). In this case, 60 kHz was chosen as the V_d frequency. Topographic artifacts from tip motion are ruled out by taking two successive PFM scans, one with V_d applied and one without, as shown in Figures 3 and 5. The voltage-off condition serves as an appropriate background measurement in which any tip motion from topography can be subtracted from the actual PFM signal. Because using the substrate or the voltage-off condition as the background signal gives consistent results, we conclude that the tip motion due to scanning does not have any noticeable effects on the measurement for either substrate.

The next possible contribution to the total force comes from electrostatic forces between the AFM probe and the substrate. These forces can come from the AFM tip or the AFM cantilever, as described by eq 3b. Contributions from the cantilever would act as parallel-plate capacitor-like interactions from the rectangular beam cantilever to the substrate. The dimensions of the cantilever used here are 125 μm × 35 μm, so any electrostatic interactions from the cantilever would be averaged over this entire area. Since Figures 3 and 5 show clear variation with submicron resolution, electrostatic interactions from the cantilever are concluded to be minimal.

Similarly, electrostatic forces from the AFM tip can contribute to the total force. This force can be written as[29]

$$F_{ES}^{Tip} = -\frac{1}{2}\frac{dC_{Tip}}{dz}\left(V_{DC} + V_{AC}\sin(\omega t) + \frac{\Delta\varphi}{q}\right)^2 \tag{4}$$

where C_{Tip}, V_{DC}, V_{AC}, ω, t, $\Delta\varphi$, and q are the tip capacitance, applied DC voltage, applied AC voltage amplitude, frequency, time, work function difference between the tip and area under the tip, and electron charge magnitude, respectively. Because the PFM experiment uses a lock-in amplifier to measure tip deflection, it is sufficient to consider only the first harmonic of eq 4, yielding

$$F_{ES,1\omega}^{Tip} \propto \left(V_{DC} + \frac{\Delta\varphi}{q}\right)V_{AC} \tag{5}$$

This relation provides multiple insights for detecting electrostatic contributions to the PR signal. To determine if electrostatic forces are significant, a DC bias sweep can be performed while measuring the resulting PR amplitude. A linear absolute-value dependence on V_{DC} with a minimum at $V_{DC} = \Delta\varphi/q$ is expected if electrostatic forces are playing a role. Figure S8 shows a piezoresponse amplitude versus V_{DC} sweep at a drive frequency of 60 kHz and V_{AC} = 8 V. The piezoresponse amplitude is independent of V_{DC} under these conditions, indicating that electrostatic effects and any differences between the workfunctions of the two materials are not significant and can be neglected.

With the elimination of the first two terms in eq 2, the PFM signal must be coming from electromechanical effects. The first effect to consider is piezoelectricity, which is what the PFM was originally designed to measure. The piezoelectric tensor for monolayer MoS_2 can be written as[11]

$$d_{ij} = \begin{bmatrix} d_{11} & -d_{11} & 0 & 0 & 0 & 0 \\ 0 & 0 & 0 & 0 & 0 & -2d_{11} \\ 0 & 0 & 0 & 0 & 0 & 0 \end{bmatrix} \tag{6}$$

where the indices correspond to those in the following definition of converse piezoelectricity

$$\varepsilon_j = d_{ij}E_i \tag{7}$$

Here, ε_j is the strain tensor employing Voigt notation and E_i is the electric field. It is important to note that the piezoelectric tensor for MoS_2 has nonzero components only within the plane of its atoms and has zero components for all out-of-plane responses. This indicates that there should be no piezoelectric effect out-of-plane. However, our experiments yield a nonzero

DOI: 10.1021/acs.nanolett.7b02123
Nano Lett. XXXX, XXX, XXX−XXX

value for d_{33}^{eff}, suggesting that this signal could be originating from the flexoelectric effect instead of the piezoelectric effect.

The converse flexoelectric tensor for MoS_2 is given by[24]

$$\mu_{mn}^{*} = \begin{bmatrix} \mu_{11}^{*} & 0 & 0 & 0 & \mu_{15}^{*} & 0 & 0 & 0 & \mu_{19}^{*} \\ \mu_{11}^{*} & 0 & 0 & 0 & \mu_{11}^{*} & 0 & 0 & 0 & \mu_{19}^{*} \\ \mu_{31}^{*} & 0 & 0 & 0 & \mu_{31}^{*} & 0 & 0 & 0 & \mu_{39}^{*} \\ 0 & 0 & 0 & 0 & 0 & \mu_{46}^{*} & 0 & \mu_{48}^{*} & 0 \\ 0 & 0 & \mu_{46}^{*} & 0 & 0 & 0 & \mu_{48}^{*} & 0 & 0 \\ 0 & \mu_{11}^{*} - \mu_{15}^{*} & 0 & \mu_{11}^{*} - \mu_{15}^{*} & 0 & 0 & 0 & 0 & 0 \end{bmatrix} \tag{8}$$

where the * indicates that the converse representation is being used and the indices are defined using the converse flexoelectric equation

$$\sigma_{ij} = \mu_{ijkl}^{*} \frac{\partial E_k}{\partial x_l} \tag{9}$$

where σ_{ij} is the stress tensor. The four indices can be transformed to two by using Voigt notation for ij, while kl follow 11 → 1, 12 → 2, 13 →3, 21 → 4, 22 → 5, 23 → 6, 31 → 7, 32 → 8, 33 → 9 to yield μ_{mn}^{*}.[24]

To a good approximation, we can assume that the electric field in the MoS_2 layer is perpendicular to the surface of the Au and thus the plane of the MoS_2 atoms. With this assumption, the contribution of the first six columns of eq 8 to the electromechanical response of MoS_2 can be neglected. Also, the first two rows describe stresses created in-plane, which will not influence the PFM measurement. Possible contributions to an out-of-plane electromechanical response from an out-of-plane electric field then include μ_{39}^{*} and μ_{48}^{*}. The former is an out-of-plane stress caused by a vertical electric field changing through the thickness of the MoS_2. The latter is an out-of-plane shear-stress mode caused by a vertical electric field varying laterally as it spreads away from the AFM tip.

In general, a superposition of both μ_{39}^{*} and μ_{48}^{*} will contribute to a measurable d_{33}^{eff} value. Although the electromechanical response can be thought of as an effective piezoelectric response, in light of the above analysis it may be more appropriate to refer to the value in this case as an effective flexoelectric response, μ_{eff}^{*}.

To obtain a rough estimate of μ_{eff}^{*} from the measured d_{33}^{eff}, the gradient $\partial E_3/\partial x_3$ is assumed to dominate and is estimated to be $2V_d/t^2$ (see Supporting Information Note 7 for details). These assumptions combined with eq 9, and $\sigma = Y\varepsilon$ where Y is Young's modulus, yield the equation

$$\mu_{\text{eff}}^{*} = \frac{\Delta z}{V_d} \cdot Y \cdot \frac{t}{2} = d_{33}^{\text{eff}} \cdot Y \cdot \frac{t}{2} \tag{10}$$

where Δz is the vertical deflection of the MoS_2. By taking Y = 270 GPa[37] and t to be a monolayer thickness of 6.5 Å,[38] our PFM measurements for MoS_2 on Au and Al_2O_3/Si yield values for μ_{eff}^{*} of 0.08 and 0.12 nC/m, respectively. These estimates are calculated from measurements only on monolayer MoS_2 and further work is needed to analyze how the flexoelectric response would respond with increasing thickness of MoS_2 (see Supporting Information Note 8).

Previous studies[15] have reported that perovskite ceramics in the paraelectric phase have a μ_{eff} on the order of 1−100 μC/m while single crystal perovskites are on the order of 1 nC/m. Values of μ_{mn} for different measurement techniques and those obtained via experiment versus theory can also vary by orders-of-magnitude but are slowly converging.

A common way to get an order of magnitude estimate of the flexoelectric coefficient of a material is to use an estimate developed by Kogan.[39] He estimates the flexocoupling coefficient with the equation

$$f \approx \frac{q}{4\pi\epsilon_0 a} \tag{11}$$

where a is the lattice constant of the material. With the definition

$$\mu \equiv \chi f \tag{12}$$

where χ is the susceptibility of MoS_2, an order of magnitude estimate of μ_{eff} can be obtained for MoS_2. Taking a = 3.2 Å[40] and χ to be $3\epsilon_0$,[41] the estimate of μ_{eff} is 0.12 nC/m. This is remarkably similar to the values derived from our experiments above.

The possibility of contamination on MoS_2 causing the measured out-of-plane electromechanical effects should not be overlooked. X-ray photoelectron spectroscopy (XPS) has been performed to detect the presence of various elements on the sample surfaces. Excess carbon, oxygen, and silicon are seen on the surface of the samples (see Supporting Information Note 9 and Table S1). Much of this is likely to be residue remaining on the surfaces after the polydimethylsiloxane (PDMS) transfer process, adventitious carbon that coats most surfaces when exposed to air, potentially other hydrocarbons, or unreacted MoO_3 precursor from the CVD process. The residue blankets the surface as it is detectable on the Au surface which contacts the PDMS but does not contain MoS_2. The substrate with residue gives little PFM signal, and the background subtraction process should remove most of the contribution to the signal generated from the residue. This does not conclusively rule out that the residue interacts differently with the MoS_2 than the substrate or that the slightly higher oxygen content on the sample affects the measurement. Further analysis is needed to definitively rule out contaminations affecting the measurement. However, the current experiment and analysis yields a strong possibility that out-of-plane flexoelectricity is present in monolayer MoS_2.

In summary, this work has shown that monolayer MoS_2 has an average measurable out-of-plane electromechanical response with a d_{33}^{eff} of 1.03 ± 0.22 pm/V on Au and 1.35 ± 0.24 pm/V on Al_2O_3/Si. There is strong evidence that its origin is from the flexoelectric effect rather than the piezoelectric effect, and an estimate of the effective flexoelectric coefficient μ_{eff}^{*} yields 0.10 nC/m. The presence of flexoelectricity in 2D materials has implications across many fields. In 2D material electronics, for example, roughness in the substrate surface could create local curvature and thus local polarization that could affect electronic device performance.[42] It also opens the door to making new types of nanoscale sensors, actuators, or energy harvesters which could be used in conjunction with piezoelectricity to enhance operation.

Methods. Monolayer MoS_2 is grown via CVD on SiO_2 from solid precursors.[43] The as-grown MoS_2 is under roughly 0.21% residual tensile strain,[44] which is released during the transfer process. A PDMS stamp and a water bath are used to separate the MoS_2 from the growth substrate. The PDMS/MoS_2 is then placed on the receiving substrate, Au/Si or Al_2O_3/Si, and

DOI: 10.1021/acs.nanolett.7b02123
Nano Lett. XXXX, XXX, XXX−XXX

heated with a hot plate to 50 °C. Slowly peeling away the PDMS transfers the MoS_2 to the substrate (see Figure S2 for details).

The Au sample is created via electron beam evaporation onto an n^{++} silicon substrate. A 5 nm titanium adhesion layer is first deposited followed by 70 nm of Au. The Al_2O_3/Si sample is fabricated by first submerging a n^{++} doped silicon substrate in 80:1 diluted HF to remove any oxide layer. The bare silicon is then immediately transferred into a Fiji ALD system. Using a trimethylaluminum precursor, a 5.3 nm thick layer of Al_2O_3 is deposited and thickness measured with a J.A. Woollam M-2000 DI ellipsometer.

Raman and PL data are taken using a Renishaw inVia Raman microscope with a 532 nm laser. PL and Raman data of the MoS_2 taken on the growth substrate, PDMS stamp, and Au sample show a clear relaxation of strain after the MoS_2 is removed from the growth substrate (see Figure S6).

PFM measurements are done on a Bruker (formerly Veeco) Dimension Icon AFM. Conductive cobalt−chromium AFM cantilevers are used (Bruker MESP-RC-V2) for PFM measurements. Tapping mode AFM images were taken using etched silicon cantilevers (Bruker TESP). A PFM drive frequency of 60 kHz and a drive amplitude of 8 V is used in all PFM measurements. See Supporting Information for more details.

■ ASSOCIATED CONTENT

Supporting Information

(PDF) The Supporting Information is available free of charge on the ACS Publications website at DOI: 10.1021/acs.nanolett.7b02123.

PFM setup, equation for d_{33}^{eff} from raw PFM Data, CVD-grown MoS_2 transfer process, MoS_2 thickness determination and optical characterization difficult, MoS_2 on Au thickness determination, MoS_2 on Al_2O_3 thickness determination, MoS_2 on SiO_2 growth substrate thickness determination, photoluminescence measurements, background subtraction for d_{33}^{eff} estimation, uncertainty estimation, voltage drop through MoS_2 on Al_2O_3, determination of drive frequency for PFM, piezoresponse amplitude vs DC bias sweep, estimating μ_{eff}^{*}, electromechanical response with increasing MoS_2thickness, XPS measurements (PDF)

■ AUTHOR INFORMATION

Corresponding Authors

*E-mail: ety@ece.utexas.edu. Phone: 512-232-5167 (E.T.Y.).
*E-mail: nanshulu@utexas.edu. Phone: 512-471-4208 (N.L.).

ORCID

Christopher J. Brennan: 0000-0001-8523-2895

Author Contributions

C.J.B. performed the sample fabrication, AFM, PFM, Raman, photoluminescence, and data analysis. R.G. and S.B. provided CVD grown MoS_2 and assisted in the transfer process. K.K. assisted in AFM measurements. N.L. and E.T.Y. assisted in project design and supervised research. C.J.B., N.L., and E.T.Y. wrote the manuscript.

Notes

The authors declare no competing financial interest.

■ ACKNOWLEDGMENTS

This work was supported by the NSF CMMI Award under Grant 1351875, NSF DMR Award under Grant 1311866, and was performed in part at the University of Texas Microelectronics Research Center, a member of the National Nanotechnology Coordinated Infrastructure (NNCI), which is supported by the National Science Foundation (Grant ECCS-1542159). E.T.Y. acknowledges the Judson S. Swearingen Regents Chair in Engineering at the University of Texas at Austin. S.K.B. acknowledges the U.S. Army Small Business Innovation Research (SBIR) Program office and the U.S. Army Research Office under Contract No. W911NF-16-C-0032. C.J.B. acknowledges Dr. Brooks Carlton Fowler Endowed Presidential Graduate Fellowship in Electrical and Computer Engineering and the Temple Foundation Graduate Microelectronic and Computer Development Fellowship in Engineering of UT-Austin. The authors acknowledge Dr. Hugo Celio for assistance in XPS measurements and Liu Wang for discussions on the calculations.

■ ABBREVIATIONS

AFM, atomic force microscopy; CVD, chemical vapor deposition; MEMS, microelectromechanical systems; PDMS, polydimethylsiloxane; PFM, piezoresponse force microscopy; PL, photoluminescence; PR, piezoresponse; TMDs, transition metal dichalcogenides; XPS, X-ray photoelectron spectroscopy

■ REFERENCES

(1) Fischetti, M. V.; Laux, S. E. *J. Appl. Phys.* **1996**, *80*, 2234−2252.
(2) Hill, E. W.; Vijayaragahvan, A.; Novoselov, K. *IEEE Sens. J.* **2011**, *11*, 3161−3170.
(3) Wang, Q. M.; Du, X. H.; Xu, B.; Cross, L. E. *IEEE Trans. Ultrason. Ferroelectr. Freq. Control* **1999**, *46*, 638−646.
(4) Xu, S.; Qin, Y.; Xu, C.; Wei, Y.; Yang, R.; Wang, Z. L. *Nat. Nanotechnol.* **2010**, *5*, 366−373.
(5) Radisavljevic, B.; Radenovic, A.; Brivio, J.; Giacometti, V.; Kis, A. *Nat. Nanotechnol.* **2011**, *6*, 147−150.
(6) Nair, R. R.; Blake, P.; Grigorenko, A. N.; Novoselov, K. S.; Booth, T. J.; Stauber, T.; Peres, N. M. R.; Geim, A. K. *Science* **2008**, *320*, 1308.
(7) Lee, G.-H.; Yu, Y.-J.; Cui, X.; Petrone, N.; Lee, C.-H.; Choi, M. S.; Lee, D.-Y.; Lee, C.; Yoo, W. J.; Watanabe, K.; Taniguchi, T.; Nuckolls, C.; Kim, P.; Hone, J. *ACS Nano* **2013**, *7*, 7931−7936.
(8) Kim, K. S. K. S.; Zhao, Y.; Jang, H.; Lee, S. Y.; Kim, J. M.; Kim, K. S. K. S.; Ahn, J.-H.; Kim, P.; Choi, J.-Y.; Hong, B. H. *Nature* **2009**, *457*, 706−710.
(9) Wu, W.; Wang, L.; Li, Y.; Zhang, F.; Lin, L.; Niu, S.; Chenet, D.; Zhang, X.; Hao, Y.; Heinz, T. F.; Hone, J.; Wang, Z. L. *Nature* **2014**, *514*, 470−474.
(10) Qi, J.; Lan, Y.-W.; Stieg, A. Z.; Chen, J.-H.; Zhong, Y.-L.; Li, L.-J.; Chen, C.-D.; Zhang, Y.; Wang, K. L. *Nat. Commun.* **2015**, *6*, 7430.
(11) Duerloo, K. A. N.; Ong, M. T.; Reed, E. J. *J. Phys. Chem. Lett.* **2012**, *3*, 2871−2876.
(12) Kim, S. K.; Bhatia, R.; Kim, T.-H.; Seol, D.; Kim, J. H.; Kim, H.; Seung, W.; Kim, Y.; Lee, Y. H.; Kim, S.-W. *Nano Energy* **2016**, *22*, 483−489.
(13) Zhu, H.; Wang, Y.; Xiao, J.; Liu, M.; Xiong, S.; Wong, Z. J.; Ye, Z.; Ye, Y.; Yin, X.; Zhang, X. *Nat. Nanotechnol.* **2014**, *10*, 151−155.
(14) Yudin, P. V.; Tagantsev, a K. *Nanotechnology* **2013**, *24*, 432001.
(15) Zubko, P.; Catalan, G.; Tagantsev, A. K. *Annu. Rev. Mater. Res.* **2013**, *43*, 387−421.
(16) Nguyen, T. D.; Mao, S.; Yeh, Y.-W.; Purohit, P. K.; McAlpine, M. C. *Adv. Mater.* **2013**, *25*, 946−974.
(17) Ahmadpoor, F.; Sharma, P. *Nanoscale* **2015**, *7*, 16555−16570.
(18) Akinwande, D.; Brennan, C. J.; Bunch, J. S.; Egberts, P.; Felts, J. R.; Gao, H.; Huang, R.; Kim, J.; Li, T.; Li, Y.; Liechti, K. M.; Lu, N.;

DOI: 10.1021/acs.nanolett.7b02123
Nano Lett. XXXX, XXX, XXX−XXX

Park, H. S.; Reed, E. J.; Wang, P.; Yakobson, B. I.; Zhang, T.; Zhang, Y.-W.; Zhou, Y.; Zhu, Y. *Extrem. Mech. Lett.* **2017**, *13*, 42−77.
(19) Dumitrică, T.; Landis, C. M.; Yakobson, B. I. *Chem. Phys. Lett.* **2002**, *360*, 182−188.
(20) Kalinin, S. V.; Meunier, V. *Phys. Rev. B: Condens. Matter Mater. Phys.* **2008**, *77*, 1−4.
(21) Kvashnin, A. G.; Sorokin, P. B.; Yakobson, B. I. *J. Phys. Chem. Lett.* **2015**, *6*, 2740−2744.
(22) Naumov, I.; Bratkovsky, A. M.; Ranjan, V. *Phys. Rev. Lett.* **2009**, *102*, 2−5.
(23) Duerloo, K.-A. N.; Reed, E. J. *Nano Lett.* **2013**, *13*, 1681−1686.
(24) Shu, L.; Wei, X.; Pang, T.; Yao, X.; Wang, C. *J. Appl. Phys.* **2011**, *110*, 104106.
(25) Zelisko, M.; Hanlumyuang, Y.; Yang, S.; Liu, Y.; Lei, C.; Li, J.; Ajayan, P. M.; Sharma, P. *Nat. Commun.* **2014**, *5*, 4284.
(26) da Cunha Rodrigues, G.; Zelenovskiy, P.; Romanyuk, K.; Luchkin, S.; Kopelevich, Y.; Kholkin, A. *Nat. Commun.* **2015**, *6*, 7572.
(27) Jungk, T.; Hoffmann, Á.; Soergel, E. *Appl. Phys. Lett.* **2007**, *91*, 253511.
(28) Jungk, T.; Hoffmann, Á.; Soergel, E. *Appl. Phys. A: Mater. Sci. Process.* **2007**, *86*, 353−355.
(29) Kalinin, S.; Bonnell, D. *Phys. Rev. B: Condens. Matter Mater. Phys.* **2002**, *65*, 125408.
(30) Yang, S. M.; Mazet, L.; Okatan, M. B.; Jesse, S.; Niu, G.; Schroeder, T.; Schamm-Chardon, S.; Dubourdieu, C.; Baddorf, A. P.; Kalinin, S. V. *Appl. Phys. Lett.* **2016**, *108*, 252902.
(31) Labuda, A.; Proksch, R. *Appl. Phys. Lett.* **2015**, *106*, 253103.
(32) Proksch, R. *J. Appl. Phys.* **2015**, *118*, 072011.
(33) Jungk, T.; Hoffmann, Á.; Soergel, E. *J. Microsc.* **2007**, *227*, 72−78.
(34) Jungk, T.; Hoffmann, A.; Soergel, E. *Appl. Phys. Lett.* **2006**, *89*, 163507.
(35) Buscema, M.; Steele, G. A.; van der Zant, H. S. J.; Castellanos-Gomez, A. *Nano Res.* **2014**, *7*, 561.
(36) Lee, C.; Yan, H.; Brus, L. E.; Heinz, T. F.; Hone, J.; Ryu, S. *ACS Nano* **2010**, *4*, 2695−2700.
(37) Bertolazzi, S.; Brivio, J.; Kis, A. *ACS Nano* **2011**, *5*, 9703−9709.
(38) Novoselov, K. S.; Jiang, D.; Schedin, F.; Booth, T. J.; Khotkevich, V. V.; Morozov, S. V.; Geim, A. K. *Proc. Natl. Acad. Sci. U. S. A.* **2005**, *102*, 10451−10453.
(39) Kogan, S. M.; et al. *Sov. Phys. Solid State* **1964**, *5*, 2069−70.
(40) Ganatra, R.; Zhang, Q. *ACS Nano* **2014**, *8*, 4074−4099.
(41) Santos, E. J. G.; Kaxiras, E. *ACS Nano* **2013**, *7*, 10741−10746.
(42) Shin, B. G.; Han, G. H.; Yun, S. J.; Oh, H. M.; Bae, J. J.; Song, Y. J.; Park, C.; Lee, Y. H. *Adv. Mater.* **2016**, *28*, 9378−9384.
(43) Liu, Y.; Ghosh, R.; Wu, D.; Ismach, A.; Ruoff, R.; Lai, K. *Nano Lett.* **2014**, *14*, 4682−4686.
(44) Lloyd, D.; Liu, X.; Christopher, J. W.; Cantley, L.; Wadehra, A.; Kim, B. L.; Goldberg, B. B.; Swan, A. K.; Bunch, J. S. *Nano Lett.* **2016**, *16*, 5836−5841.

DOI: 10.1021/acs.nanolett.7b02123
Nano Lett. XXXX, XXX, XXX−XXX

Supporting Information

Out-of-Plane Electromechanical Response of Monolayer Molybdenum Disulfide Measured by Piezoresponse Force Microscopy

Christopher J. Brennan[1,2], Rudresh Ghosh[1,2], Kalhan Koul [1,2], Sanjay K. Banerjee[1,2,3], Nanshu Lu[1,2,3,4,5], Edward T. Yu[1,2,3]**

[1]Microelectronics Research Center, University of Texas at Austin, Austin, TX 78758

[2]Deparment of Electrical and Computer Engineering, University of Texas at Austin, Austin, TX 78701 USA.

[3]Texas Materials Institute, University of Texas at Austin, Austin, TX 78712 USA

[4]Center for Mechanics of Solids, Structures and Materials, Department of Aerospace Engineering and Engineering Mechanics, University of Texas at Austin, Austin, TX 78712 USA

[5]Department of Biomedical Engineering, University of Texas at Austin, Austin, TX 78712 USA

* Corresponding authors:

Edward T. Yu, ety@ece.utexas.edu, 512-232-5167, MER 1.206M, 10100 Burnet Rd. Bldg 160, Austin, TX 78758

Nanshu Lu, nanshulu@utexas.edu, 512-471-4208, 210 E. 24th St, Austin, TX 78712

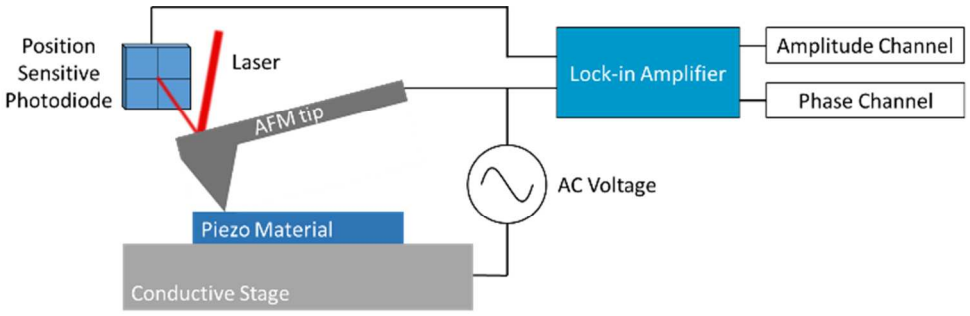

Figure S1. A schematic showing the PFM process and the tip sample geometry. An AC voltage is applied across the material to be measured. The AC voltage is also routed to a lock-in amplifier which uses its frequency as the reference frequency. The AC voltage causes a corresponding alternating expansion and contraction in the piezoelectric material which is measured as a laser deflection in a position sensitive photodiode (PSD). This signal is fed into the lock-in amplifier and the frequency component at the reference frequency is amplified. The lock-in amplifier outputs two different channels, the amplitude and phase of the amplified signal.

Supporting Note 1: *Equation for* d_{33}^{eff} *From Raw PFM Data*

The d_{33}^{eff} values given in this paper required processing from the raw data captured by the PFM. Two channels of data are captured in a PFM measurement: the piezoresponse amplitude and the piezoresponse phase (see Figure S1). The piezoresponse amplitude channel is captured as a voltage produced by laser movement on a position sensitive photodiode. The voltage is then converted into physical deflection by measuring the deflection sensitivity, s_d, of the AFM cantilever. This is done by measuring how much the laser is deflected in the PSD for a known vertical movement. Also during the PFM measurement, a hardware gain of 16x is used to enhance the signal. Based on these factors d_{33}^{eff} is then given by

$$d_{33}^{eff} = \frac{(PR\ AMP)\cdot s_d}{V_d \cdot GAIN}. \quad \text{(S1)}$$

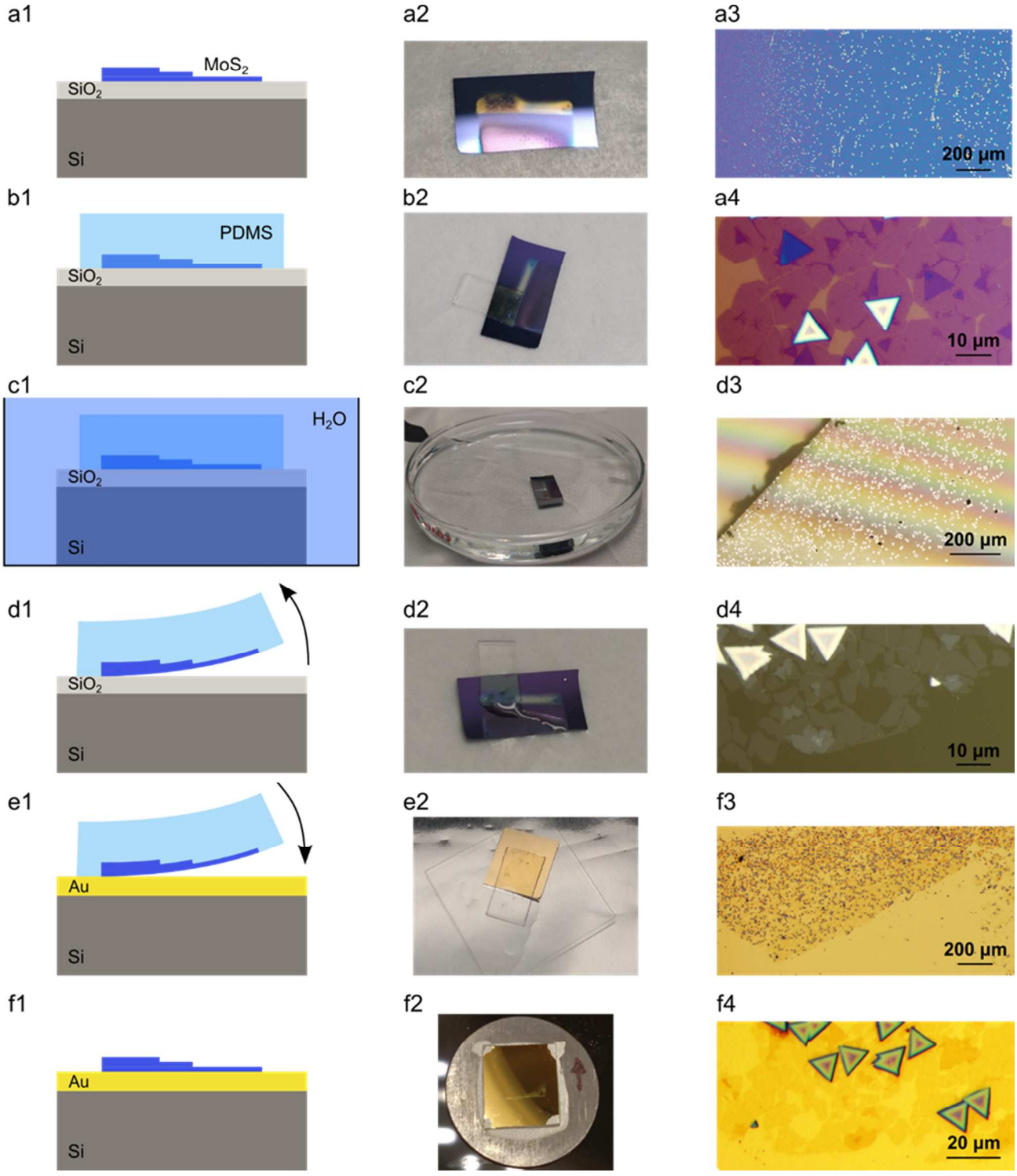

Figure S2. The transfer process of CVD grown MoS_2 is shown schematically in (**a1-f1)** and pictorially in (**a2-f2)**. The process flow is as follows: (**a1**) MoS_2 is grown on SiO_2 via CVD, (**b1**) a PDMS stamp is pressed on the MoS_2, (**c1**) the sample is submerged in water, (**d1**) the sample is removed from water,

dried, and the PDMS is peeled off with some MoS_2, (**e1**) the MoS_2 on PDMS is placed on the receiving substrate, gold shown here, and heated on a hot plate to 50 °C, (**f1**) finally the PDMS stamp is slowly peeled away, leaving the MoS_2 on the receiving substrate. Microscope images at two different magnifications show the MoS_2 on the growth substrate (**a3-4**), on the PDMS stamp (**d3-4**), and on the gold substrate (**f3-4**). Due to the PDMS being soft, strain from bending can cause cracking of the MoS_2 during the transfer process. This type of damage will not affect our PFM measurements.

Supporting Note 2: *MoS_2 Thickness Determination and Optical Characterization Difficulty*

AFM step height measurements on 2D materials have been shown to be somewhat unreliable and dependent on AFM measurement conditions[1,2]. This is exacerbated if the 2D material and its substrate have different mechanical properties[3–5]. Additionally, obtaining step-height measurements on substrates which have a roughness on the order of the film thickness is difficult. We have also seen slight variation between different AFM measurements of the same sample. Despite this, we believe that we have reasonably confirmed that we are measuring monolayer MoS_2 on both substrates.

Figure S3 shows MoS_2 on gold. The AFM height profile shown in Figure S3b reveals that the MoS_2 measured in Figure 3 of the main text is monolayer. The Raman data in Figure S3d further confirms the presence of monolayer MoS_2, with an $A_{1g} - E^1_{2g}$ ($A'_1 - E'$) peak separation of 19.7 cm^{-1}. The photoluminescence (PL) data (Figure S3e) also shows a significantly higher intensity on the monolayer region than on the multilayer region.

The thickness of MoS_2 on Al_2O_3 is more difficult to characterize. Figure S4a shows a tapping mode AFM image of the sample measured with PFM in Figure 5. The monolayer step shows a height value thicker than expected for a monolayer. Different literature reports have shown that 2D material step height measurements can be somewhat unreliable[1,2] and can be affected by differences in the mechanical properties of the 2D material and its substrate[3–5]. These issues are often solved by preforming Raman and PL measurements to confirm the presence of monolayer MoS_2. This is unfortunately not possible in our

sample because these two techniques give very weak signals when on such a thin layer of Al_2O_3 on silicon.

The sample geometry does not allow enough light to be absorbed by the MoS_2 to give measurable Raman and PL data, as is indicated by the poor optical contrast in the optical microscope image in Figure 1. Typically, thicker dielectric layers create internal reflections of light that allow for an increased optical contrast and absorption of light in the 2D materials[4]. MoS_2 directly placed on a silicon substrate does not absorb enough light (and emission is quenched) to give a measurable Raman and PL signal[6]. Also, a recent study has shown that for the thickness of Al_2O_3 used in this paper (~5.3 nm), MoS_2 is expected to have a very poor optical contrast[7]. With this understanding, it is expected that the Raman and PL signals of thin MoS_2 on 5.3 nm Al_2O_3 on silicon will be weak. Thicker regions of MoS_2 that are optically visible do give a measurable signal, as shown in Figure 2. Other studies showing Raman and PL of MoS_2 on sapphire and thin Al_2O_3 seem to mostly be on bulk sapphire[8] or sufficiently thick (~50 nm) Al_2O3_3 to offer optical contrast in microscope images[7].

To overcome this, we characterize the MoS_2 remaining on the SiO_2 growth substrate after the transfer process. Figure S5 shows that the MoS_2 on the growth SiO_2 also shows slightly inflated thickness values as measured by the AFM. However, Raman data (Figure S5e) confirms that this area of MoS_2 is monolayer. The thickness of monolayer MoS_2 measured on the growth substrate and after being transferred to the Al_2O_3 is comparable. Also, no thinner areas of MoS_2 on Al_2O_3 or SiO_2 are found across the samples. In the calculation done in this work, the thickness of monolayer MoS_2 is chosen to be 0.65 nm because this has been agreed upon in the literature as the thickness of pristine MoS_2. Any deviations from this value measured by AFM in this paper are attributed to errors in the AFM measurement.

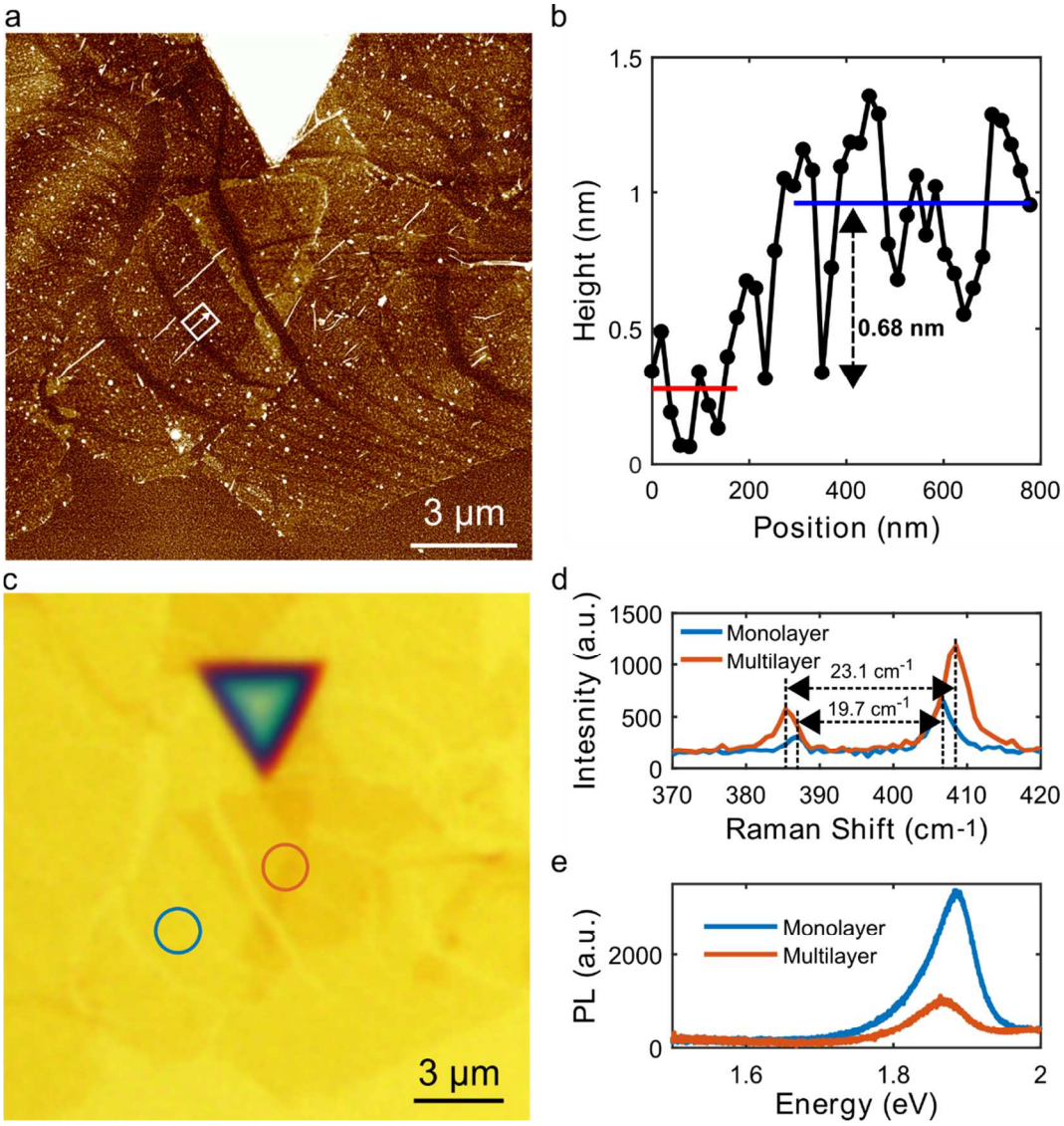

Figure S3. Tapping mode AFM image of MoS_2 on the gold substrate is shown in (**a**). A height profile is given for the white box in (**a**) where the width of the box indicates the area averaged to obtain (**b**). An optical microscope image is shown in (**c**). The blue and orange circles represent monolayer and multilayer MoS_2 measurement locations for Raman spectroscopy (**d**) and photoluminescence (**e**) measurements.

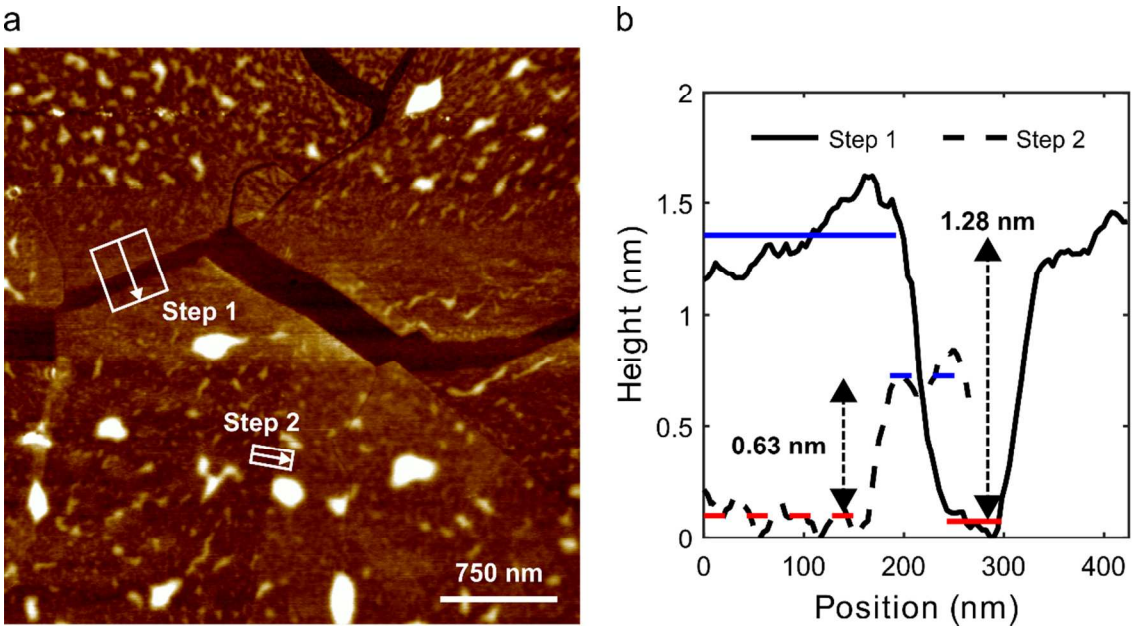

Figure S4. A tapping mode AFM image taken of the MoS_2 on Al_2O_3 sample a few months after the PFM measurement taken in Figure 5 is shown in (**a**). (**b**) shows step height profiles for the two boxes highlighted in (**a**). Step 1 shows a step from monolayer MoS_2, to the Al_2O_3 substrate, to another monolayer region. The AFM height is inflated from the expected monolayer thickness and is attributed to scanning over materials with different mechanical properties. Step 2 shows a monolayer to bilayer MoS_2 step with an expected thickness value.

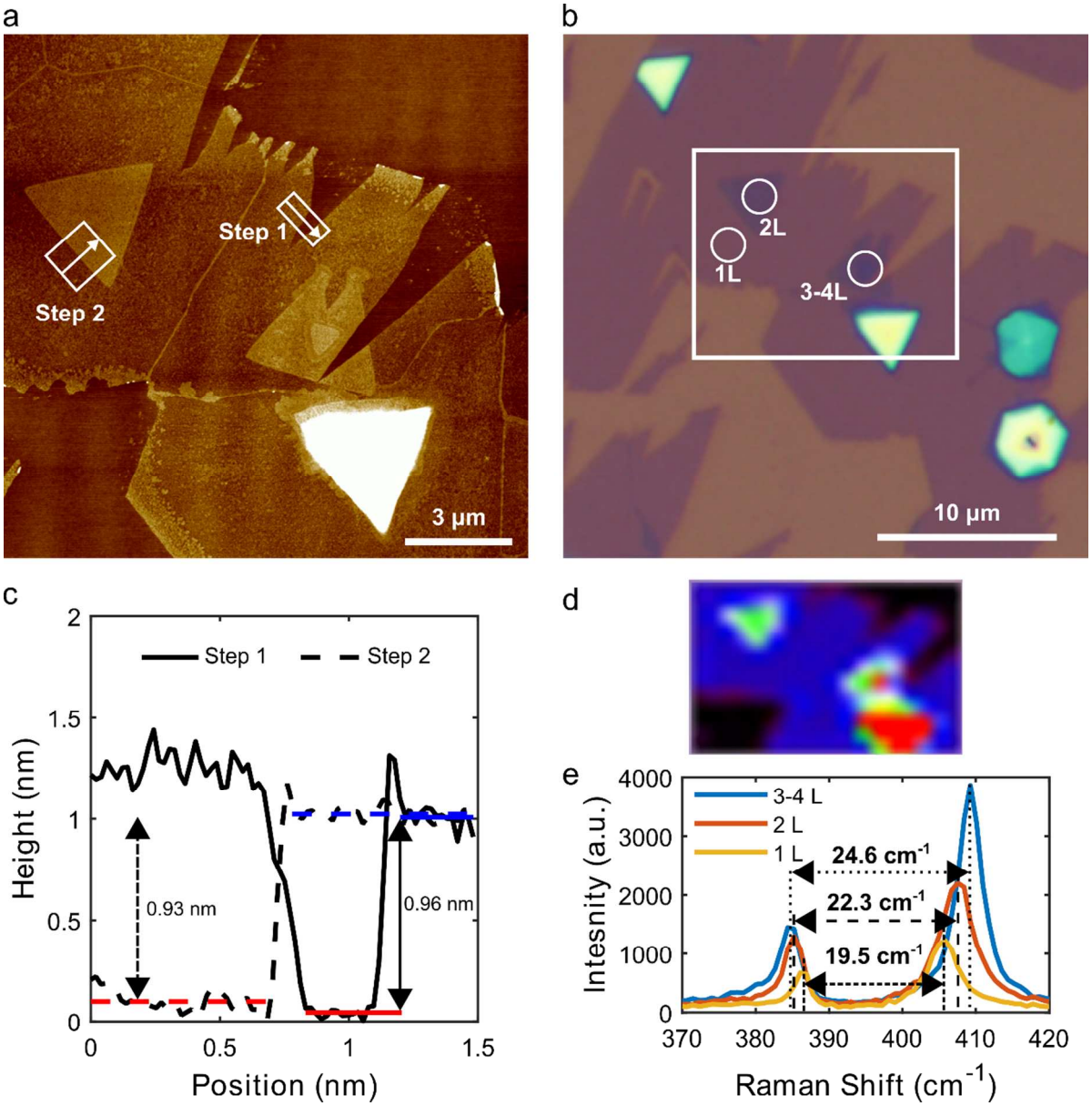

Figure S5. A tapping mode AFM image is shown in (**a**) with boxes representing areas in which step height measurements are taken and displayed in (**c**). An optical image is shown in (**b**), where the white box represents the area shown in (**d**) and depicts a color-coded Raman map. The color corresponds to the integrated intensity of the A_{1g} MoS_2 peak to the silicon peak at 520 cm^{-1}. As expected, the signal becomes stronger as thicker MoS_2 is measured. Raman spectra of the points circled in (**b**) are shown in (**e**). This confirms the presence of monolayer MoS_2.

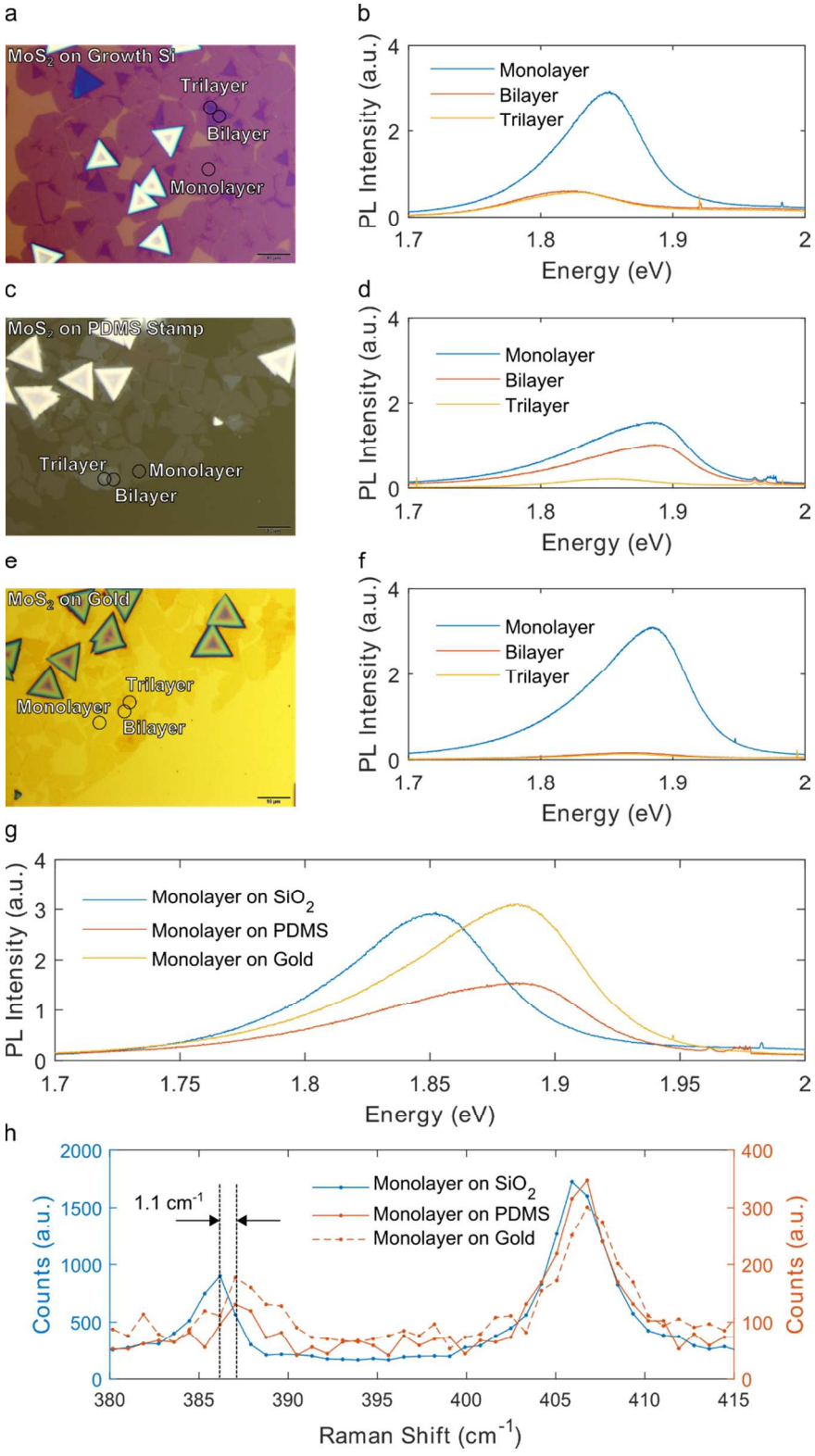

Figure S6. Microscope images of the MoS_2 on the growth substrate (**a**), PDMS stamp (**c**), and gold (**e**), with corresponding photoluminescence measurements (**b,d,f**). As expected, the monolayer MoS_2 has the

highest PL intensity because of its transition to a direct-gap semiconductor at the monolayer limit. PL and Raman data from the MoS_2 on the different substrates are shown together in (**g**) and (**h**), respectively, to show the peak shifts. The substrate can affect the peak locations on the PL signal[4], so PL alone is not reliable to determine strain. The E^1_{2g} Raman peak is sensitive to strain and can be used to estimate the amount of residual biaxial strain present in the MoS_2 while on the growth substrate of SiO_2[9]. With a shift of roughly 1.1 cm^{-1} in the E^1_{2g}, we estimate a residual tensile strain of 0.21 %.

Supporting Note 3: *Background Subtraction for d_{33}^{eff} Estimation*

Although **eq S1** is strictly correct, a background signal is always present regardless of the material that is being measured. To remove this background signal, which may be cantilever, sample, or PFM dependent, a background subtraction process is implemented which uses both the piezoresponse amplitude and piezoresponse phase channels.

First, a PFM image that includes monolayer MoS_2 and the exposed substrate is taken with the drive voltage (V_d) applied. Immediately following this, a second PFM image is taken without applying V_d to the sample. This allows for two different types of background measurements: one that measures the response of the substrate, and one that measures the error introduced by any tip motion during the scanning process or from the feedback electronics.

Second, values of the piezoresponse amplitude and piezoresponse phase for each material are gathered by averaging over areas that contain either monolayer MoS_2, exposed substrate, or any area for the V_{off} PFM image (there are no distinguishable differences in the piezoresponse amplitude or phase signal on the MoS_2 and substrate when V_d is not applied).

Vectors can now be constructed from the piezoresponse amplitude and piezoresponse phase measurements taken on the MoS_2, substrate, and V_{off} image. A background-subtracted piezoresponse amplitude estimate is then obtained by performing a vector subtraction of the background signal vector from the MoS_2 signal vector. The new piezoresponse amplitude of the background-subtracted vector is used in **eq S1** to estimate d_{33}^{eff}. This process is illustrated schematically in Figure 4.

The same subtraction procedure is applied with the MoS_2 and V_{off} vectors to obtain another estimate of d_{33}^{eff}. If there is little contribution to the signal measured on the MoS_2 by the substrate, the MoS_2-substrate and MoS_2-V_{off} d_{33}^{eff} estimates should be similar, which is indeed the case. Lastly, the contribution to the piezoresponse signal by the substrate can be estimated by doing a substrate-V_{off} vector subtraction. This yields order-of-magnitude smaller values than on the MoS_2, suggesting that the substrates used in this experiment are not responding electromechanically in the PFM measurements.

Supporting Note 4: *Uncertainty Estimation*

The uncertainty in the d_{33}^{eff} measurement is calculated by using error propagation of the measured values. To do this an equation must be created which incorporates all variables containing uncertainty. In this case, the equation for d_{33}^{eff} is

$$d_{33}^{eff} = \frac{S_d}{V_d \cdot g} \left|\overrightarrow{A^{BS}}\right|, \tag{S2}$$

where $\left|\overrightarrow{A^{BS}}\right|$ is the amplitude, in mV, of the background subtracted vector. $\left|\overrightarrow{A^{BS}}\right|$ can be expanded in terms of the measured values as

$$\left|\overrightarrow{A^{BS}}\right| = \sqrt{\left|\overrightarrow{A^{M}}\right|^2 + \left|\overrightarrow{A^{B}}\right|^2 - 2\left|\overrightarrow{A^{M}}\right|\left|\overrightarrow{A^{B}}\right|\cos(\theta^M - \theta^B)}\,, \tag{S3}$$

where $\left|\overrightarrow{A^{M}}\right|$, θ^M, $\left|\overrightarrow{A^{B}}\right|$, and θ^B are the amplitude and phase of the vector measured on the MoS_2 and background, respectively.

The uncertainty of $\left|\overrightarrow{A^{BS}}\right|$ can be obtained by using the formula

$$\sigma_{A-BS} = \sqrt{\left(\frac{\partial\left|\overrightarrow{A^{BS}}\right|}{\partial\left|\overrightarrow{A^{M}}\right|}\right)^2 \sigma_{AM}^2 + \left(\frac{\partial\left|\overrightarrow{A^{BS}}\right|}{\partial\left|\overrightarrow{A^{B}}\right|}\right)^2 \sigma_{AB}^2 + \left(\frac{\partial\left|\overrightarrow{A^{BS}}\right|}{\partial\theta^M}\right)^2 \sigma_{PM}^2 + \left(\frac{\partial\left|\overrightarrow{A^{BS}}\right|}{\partial\theta^B}\right)^2 \sigma_{PB}^2}\,, \tag{S4}$$

where σ_{AM}, σ_{AB}, σ_{PM}, σ_{PB}, are the uncertainties associated with the amplitude of the MoS_2 and background, and the phase of the MoS_2 and background, respectively. The values for the measured amplitudes and phases are obtained by performing a Gaussian fit over a distribution of points in the PFM measurement to find a mean value. The associated uncertainties are taken to be the 95% confidence interval of the fitted mean values. All calculations are done using MATLAB.

Next, the error must be propagated through **eq S2**. This can be done by using the equation

$$\sigma_d = d_{33}^{eff}\sqrt{\left(\frac{\sigma_s}{s_d}\right)^2 + \left(\frac{\sigma_V}{V_d}\right)^2 + \left(\frac{\sigma_{A-BS}}{\left|\overrightarrow{A^{BS}}\right|}\right)^2}, \tag{S5}$$

where σ_d, σ_s, and σ_V, are the uncertainties associated with d_{33}^{eff}, s_d, and V_d, respectively.

This value represents the uncertainty in the fitting of the mean value of the measurements. To incorporate any uncertainty originating from the substrate on the measurement, the d_{33}^{eff} calculated when comparing the substrate to the V_{off} condition can be thought of an error estimate. The total uncertainty can then be calculated as

$$\sigma_{tot} = \sqrt{{\sigma_d}^2 + {d_{33,sub-Voff}^{eff}}^2}. \tag{S6}$$

In **Table 1**, the calculated d_{33}^{eff} and σ_{tot} are shown for background subtraction of MoS_2 versus the substrate, MoS_2 versus the V_{off} condition, and d_{33}^{eff} and σ_d for comparing the substrate versus the V_{off} condition.

Supporting Note 5: *Voltage drop through MoS_2 on Al_2O_3*

Assuming that the electric flux density through the two materials is equal, we have

$$\epsilon_{MoS_2} E_{MoS_2} = \epsilon_{Al_2O_3} E_{Al_2O_3}. \tag{S7}$$

The electric field is given by

$$E_i = -\frac{V_i}{t_i} \tag{S8}$$

where t is the thickness of the material. Combining **eq S7** and **eq S8**, we obtain

$$\epsilon_{MoS_2} \frac{V_{MoS_2}}{t_{MoS_2}} = \epsilon_{Al_2O_3} \frac{V_{Al_2O_3}}{t_{Al_2O_3}}. \tag{S9}$$

Now, by using

$$V_{MoS_2} + V_{Al_2O_3} = V_d, \tag{S10}$$

where V_d is the drive voltage, we can obtain

$$V_{MoS_2} = V_d \frac{\epsilon_{Al_2O_3}/t_{Al_2O_3}}{\epsilon_{MoS_2}/t_{MoS_2} + \epsilon_{Al_2O_3}/t_{Al_2O_3}}. \tag{S11}$$

Supporting Note 6: *Determination of Drive Frequency for PFM*

The piezoresponse amplitude of the PFM measurement is in general frequency dependent. A typical frequency sweep of the piezoresponse amplitude on the MoS_2/gold sample is shown in Figure S7. This frequency dependence should not be of electromechanical origin, but instead is most likely caused by the measurement electronics. Similar frequency dependencies are seen with different cantilevers, different substrates, and when the drive voltage is not routed to the sample. This is another reason for doing a PFM measurement without applying the drive voltage to obtain a background signal.

The drive frequency used in the measurements must be away from the extraneous peaks in the piezoresponse amplitude frequency sweep as well as away from the clamped mechanical resonance point of the cantilever (roughly 800 kHz). The frequency 60 kHz is chosen because it is within a frequency independent region in the frequency sweep.

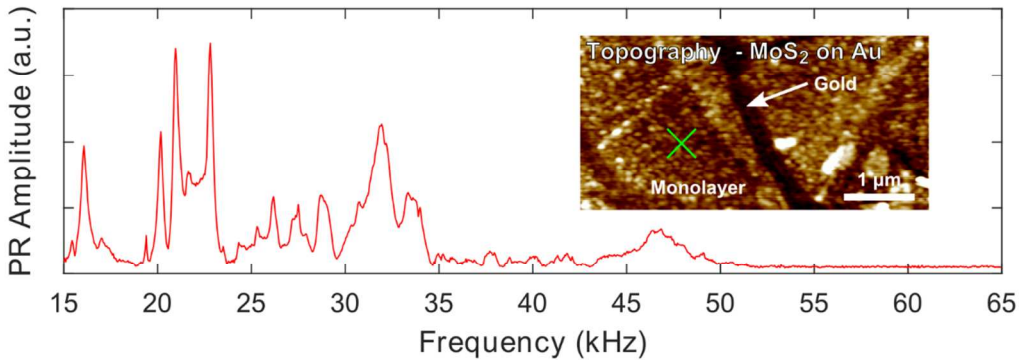

Figure S7. The PR amplitude vs drive voltage frequency measured on the MoS_2 on gold sample. The location of the measurement is denoted by the 'x' in the inset AFM topographic image. A chaotic relationship is seen at the lower frequencies, but at higher frequencies the PR amplitude becomes independent of frequency. 60 kHz is used in all PFM measurements to be well within the frequency independent region. These frequencies are well below the contact resonant point of the AFM cantilever.

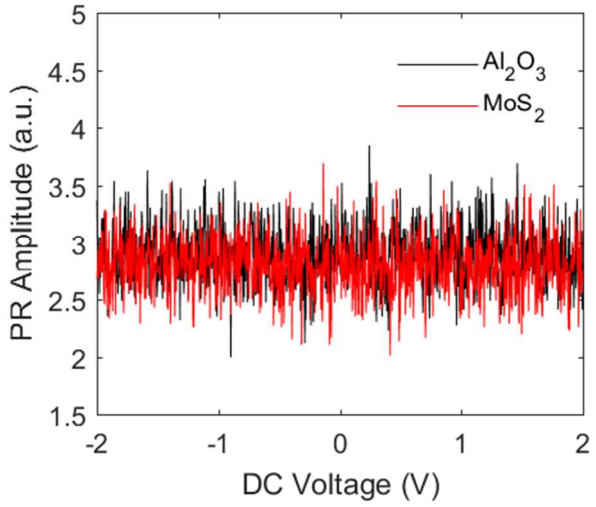

Figure S8. The PR amplitude measured as the DC voltage between the AFM tip and n^{++} Si is swept on the MoS_2 / Al_2O_3 sample. Measurements on both the MoS_2 and the Al_2O_3 show that the PR amplitude is independent from the DC voltage. This indicates that the electrostatic interactions and work-function differences are not significant.

Supporting Note 7: *Estimating* μ_{eff}^{*}

To estimate μ_{eff}^{*}, let us first better understand **eq 7** and **eq S1**. By doing a PFM measurement, converse piezoelectricity is used to effectively measure the strain caused by an applied electric field. Using the definition of strain,

$$\varepsilon_3 = \frac{\Delta z}{t}, \tag{S12}$$

where *Δz* is the vertical deflection measured by the PFM (piezoresponse amplitude) and *t* is the thickness of the material being measured, **eq 7** can be written as

$$d_{33}^{eff} = \frac{\Delta z}{tE_3}. \tag{S13}$$

This is similar to **eq S1** where *Δz* contains the deflection sensitivity and the gain factor, and therefore represents the actual deflection of the sample.

Now consider the different components in **eq 9** which may be present in MoS_2 if we assume that the electric field is perpendicular to the surface of the gold and MoS_2:

$$\sigma_1 = \mu_{19}^{*}\frac{\partial E_3}{\partial x_3}, \tag{S14a}$$

$$\sigma_2 = \mu_{19}^{*}\frac{\partial E_3}{\partial x_3}, \tag{S14b}$$

$$\sigma_3 = \mu_{39}^{*}\frac{\partial E_3}{\partial x_3}, \tag{S14c}$$

$$\sigma_4 = \mu_{48}^{*}\frac{\partial E_3}{\partial x_2}, \tag{S14d}$$

$$\sigma_5 = \mu_{48}^{*}\frac{\partial E_3}{\partial x_1}. \tag{S14e}$$

Of these components, σ_1 and σ_2 will create in-plane stress which may or may not create out-of-plane displacement due to Poisson-like effects. In **eq S14d** and **eq S14e**, the out-of-plane shear stress contributions σ_4 and σ_5 could create contributes to measured out-of-plane displacement. The most likely out-of-plane displacement would be due to **eq S14c** where an out-of-plane electric field changing in the z-

direction causes stress is the z-direction. This is plausible because the gradient is taken over the very short distance of a single monolayer of MoS_2.

For simplicity, we assume that the geometry and response of the system is approximated by **eq S14c** and substitute μ_{eff}^{*} for μ_{39}^{*}. Next, we assume that the dominant electric field derivative term, $\partial E_3/\partial x_3$, can be approximated, at these small length scales, as $\partial E_3/\partial x_3 \approx 2V_d/t^2$. This assumption corresponds to a linear dependence of E_3 on x_3, and a quadratic dependence of the electrostatic potential on x_3, within the MoS_2 layer, subject to the boundary conditions that E_3 vanish in the metal tip and sample contact, and that the total potential drop across the MoS_2 layer be V_d. Finally, using $\sigma = Y\varepsilon$ and **eq S13**, **eq 9** can be rewritten as

$$\mu_{eff}^{*} = \frac{\Delta z}{V_d} \cdot Y \cdot \frac{t}{2} = d_{33}^{eff} \cdot Y \cdot \frac{t}{2}. \quad \text{(S17)}$$

Assuming Y = 270 GPa and t = 0.65 nm for monolayer MoS_2, **eq S17** yields 0.08 nC/m and 0.12 nC/m, based on PFM measurements for MoS_2 on gold and Al_2O_3/Si, respectively. This serves only as an order-of-magnitude estimate of μ_{eff}^{*}.

Supporting Note 8: *Electromechanical Response with Increasing MoS_2 Thickness*

Detailed analysis of the effect of thickness on the calculations is beyond the scope of this paper, but should be addressed briefly. Piezoelectricity does depend on the number of layers present as shown in literature[10,11]. Few-, odd-number layers of MoS_2 have a symmetry such that no inversion symmetry point is present, resulting in in-plane piezoelectricity. Even-layered MoS_2, on the other hand, has a different symmetry which has an inversion symmetry point and is thus not piezoelectric. Additionally, as the number of odd-layers increases to 3, 5, 7, etc., the in-plane MoS_2 can increasingly be considered 'bulk' which is not piezoelectric. The result is a stark decrease in the piezoelectric response as the number of layers increase, as is confirmed in references[10,11]. It should be emphasized that regardless of the number of layers present, these piezoelectric responses are only within the plane of the MoS_2 film.

Flexoelectricity is more difficult to analyze with increasing thickness. As MoS_2 transitions from odd-number to even-number layer, its point group changes from D_{3h} to D_{3d}, respectively. The resulting flexoelectric tensors are different from each other[12], but still have non-zero out-of-plane coefficients, namely μ^*_{39}. These differences make it more difficult to directly compare even- and odd-numbered layers of MoS_2 by using the PFM technique, especially since we are grouping the total response into the effective value μ^*_{eff}. Moreover, our estimates for μ^*_{eff} rely on estimates of the electric field distribution throughout the thickness of MoS_2. This field distribution will certainly change with increasing layer thickness and is beyond the scope of this paper to calculate. These issues are a subject of ongoing investigation and may be the subject of a future publication.

Supporting Note 9: *XPS Measurements*

XPS measurements were performed to look for surface contaminants that could affect the PFM signal. Three separate samples were measured: 1) the MoS_2 on gold sample for which PFM images are shown in Figure 3**,** 2) gold deposited on an Si/SiO_2 substrate, 3) gold deposited on an Si/SiO_2 substrate that was stamped by PDMS without MoS_2. **Supporting Table S1** shows the concentration of various elements detected on the surfaces of the samples.

A notable amount of carbon is detected on all of the samples, most of which is probably from adventitious carbon which is found on all samples exposed to air. The samples which were stamped with PDMS show increased levels of oxygen and silicon compared to the non-stamped gold sample. Residue left on the sample from the stamping process, or unreacted MoO_3 from the CVD growth processes most-likely is the culprit of the increase. Since the silicon and oxygen increase is also seen on the gold sample without the MoS_2, it is assumed that any PDMS residue is blanket-deposited wherever the PDMS contacts and does not preferably attach to the MoS_2. This means that if the PDMS residue contributes to the PFM signal, its contribution to the MoS_2 signal can be removed by doing the background subtraction process of the substrate/residue PFM measurement. One possible complication would be if the PDMS residue

interacts differently with the MoS_2 versus the gold or Al_2O_3 substrates. More work is needed to rule out any such effects.

We also note that the typical magnetic lens used for XPS measurements could not be used for the MoS_2/gold sample because it was mounted on a magnetic AFM disk for better electrical contact during PFM measurements. Only the electrostatic lens was used for this sample, so the % concentration values may not be precise and represent a broader range of possible percentages.

Table S1. Percent concentration of selected elements on the surface of three different samples using XPS.

Element	Gold Only	PDMS-Stamped Gold	MoS_2 on Gold
Au	62.0 %	56.4 %	37.3 %
C	34.2 %	35.2 %	39.0 %
O	3.8 %	6.0 %	16.1 %
Si	0 %	2.4 %	5.6 %
Mo	0 %	0 %	0.9 %
S	0 %	0 %	1.1 %

References

(1) Shearer, C. J.; Slattery, A. D.; Stapleton, A. J.; Shapter, J. G.; Gibson, C. T. *Nanotechnology 27*, 0.

(2) Nemes-Incze, P.; Osváth, Z.; Kamarás, K.; Biró, L. P. *Carbon N. Y.* **2008**, *46*, 1435–1442.

(3) Castellanos-Gomez, A.; Roldán, R.; Cappelluti, E.; Buscema, M.; Guinea, F.; van der Zant, H. S. J.; Steele, G. a. *Nano Lett.* **2013**, *13*, 5361–5366.

(4) Buscema, M.; Steele, G. A.; van der Zant, H. S. J.; Castellanos-Gomez, A. *Nano Res.* **2014**, *7*, 561–571.

(5) Brennan, C. J.; Nguyen, J.; Yu, E. T.; Lu, N. *Adv. Mater. Interfaces* **2015**, *2*, 1500176.

(6) Man, M. K. L.; Deckoff-Jones, S.; Winchester, A.; Shi, G.; Gupta, G.; Mohite, A. D.; Kar, S.; Kioupakis, E.; Talapatra, S.; Dani, K. M. *Sci. Rep.* **2016**, *6*, 20890.

(7) Bhattacharjee, S.; Ganapathi, K. L.; Chandrasekar, H.; Paul, T.; Mohan, S.; Ghosh, A.; Raghavan, S.; Bhat, N. *Adv. Electron. Mater.* **2017**, *3*, 1–9.

(8) Dumcenco, D.; Ovchinnikov, D.; Marinov, K.; Lazić, P.; Gibertini, M.; Marzari, N.; Sanchez, O. L.; Kung, Y.-C.; Krasnozhon, D.; Chen, M.-W.; Bertolazzi, S.; Gillet, P.; Fontcuberta i Morral, A.; Radenovic, A.; Kis, A. *ACS Nano* **2015**, *9*, 4611–4620.

(9) Lloyd, D.; Liu, X.; Christopher, J. W.; Cantley, L.; Wadehra, A.; Kim, B. L.; Goldberg, B. B.; Swan, A. K.; Bunch, J. S. *Nano Lett.* **2016**, *16*, 5836–5841.

(10) Wu, W.; Wang, L.; Li, Y.; Zhang, F.; Lin, L.; Niu, S.; Chenet, D.; Zhang, X.; Hao, Y.; Heinz, T. F.; Hone, J.; Wang, Z. L. *Nature* **2014**, *514*, 470–474.

(11) Zhu, H.; Wang, Y.; Xiao, J.; Liu, M.; Xiong, S.; Wong, Z. J.; Ye, Z.; Ye, Y.; Yin, X.; Zhang, X. *Nat. Nanotechnol.* **2014**, *10*, 151–155.

(12) Shu, L.; Wei, X.; Pang, T.; Yao, X.; Wang, C. *J. Appl. Phys.* **2011**, *110*, 104106.